Geologica Acta, Vol.16, Nº 2, June 2018, 215-235
DOI: 10.1344/GeologicaActa2018.16.2.6

geologica acta

Seismic imaging and attribute analysis of Chicxulub Crater central sector, Yucatán Platform, Gulf of Mexico

I. CANALES-GARCÍA[1,2] **J. URRUTIA-FUCUGAUCHI**[2*] **E. AGUAYO-CAMARGO**[3]

[1]**Posgrado en Ciéncias del Mar y Limnología, Universidad Nacional Autónoma de México**
Ciudad Universitaria, Delegación Coyoacán, 04510 México, México

[2]**Programa Universitario de Perforaciones en Océanos y Continentes, Instituto de Geofísica, Universidad Nacional Autónoma de México, Departamento de Geomagnetismo y Exploración**
Ciudad Universitaria, Delegación Coyoacán, 04510 México, México. Urrutia-Fucugauchi E-mail: juf@geofisica.unam.mx

[3]**Facultad de Ingeniería, Universidad Nacional Autónoma de México, Departamento de Geología**
Ciudad Universitaria, Delegación Coyoacán, 04510 México, México

*Corresponding author

ABSTRACT

Chicxulub Crater, formed ~66Ma ago by an asteroid impact on the southern Gulf of Mexico, is the best preserved of the three large multi-ring basins in the terrestrial record. The crater structure is characterized by a semi-circular concentric ring pattern, marking the crater basin, peak ring, terrace zone and basement uplift. Analysis of a grid of 19 seismic reflection profiles using seismic attributes, marker horizons, contour surfaces and 3-D views is used to investigate the stratigraphy of the central zone. We used interactive software and routine applications to map the impact breccias, breccia-carbonate contact and post-impact carbonates. Four horizons marked by high-amplitude reflectors representing high-impedance contrasts were identified and laterally correlated in the seismic images. Complex trace attribute analysis was applied for petrophysical characterization. Surface contour maps of base and top of stratigraphic packages were constructed, which mapped the impactites and post- and pre-impact carbonate stratigraphy. Basin floor, marked by the contact between the impact breccias and overlying carbonates is shown by laterally discontinuous high-amplitude reflectors. Discontinuous scattered reflectors interpreted as the upper breccias beneath the crater floor, have an average thickness of ~300msm. The Paleogene sedimentary units are characterized by multiple reflectors with lateral continuity, which contrast with the seismic response of underlying breccias. The basal Paleocene sediments follow the basin floor relief. Upwards in the section, the carbonate strata are characterized by horizontal reflectors, which are interrupted by a regional unconformity. Onlap/downlap packages over the unconformity record a period of sea level change.

KEYWORDS | **Chicxulub Crater. Structure. Stratigraphy. Seismic attributes. Yucatán Platform. Gulf of Mexico.**

INTRODUCTION

The Chicxulub Crater formed by an asteroid impact on the Yucatán carbonate Platform in the southern Gulf of Mexico (Fig. 1) (Hildebrand *et al.*, 1991, 1998; Sharpton *et al.*, 1992). The impact is linked to the end Cretaceous mass extinction, marking the Cretaceous/Paleogene (K/Pg) boundary (Alvarez *et al.*, 1980; Schulte *et al.*, 2010). The crater has a multi-ring morphology characterized by a peak ring and central basement uplift, with a diameter of ~200km. After formation, the crater was covered by carbonate sediments; there are presently no surface outcrops of ejecta and crater structures. The buried crater was first identified in oil exploration surveys, from the semi-circular concentric gravity and magnetic anomaly patterns in northern Yucatán Peninsula (Penfield and Camargo-Zanoguera, 1981). Studies of impact dynamics and cratering require data on crater structure, central uplift, peak ring, crater rim, terraces, fault zones, melt rocks and breccias. Geophysical surveys have focused on crater structure, cratering, ejecta deposits, impact effects and impact dynamics (Hildebrand *et al.*, 1991, 1998; Sharpton *et al.*, 1993; Morgan *et al.*, 1997; Gulick *et al.*, 2008, 2013; Schulte *et al.*, 2010; Urrutia-Fucugauchi *et al.*, 2011). Understanding multi-ring forming impacts is a major research area in planetary sciences (Melosh, 1989; Pierazzo and Melosh, 2000; Urrutia-Fucugauchi and Pérez-Cruz, 2009, 2016).

The Yucatán Platform extends areally ~300,000km^2, separating the Caribbean Sea from the Gulf of Mexico. This platform has developed on a continental block of Pan-African affinity from accumulation of calcareous material deposited on crystalline basement since the middle Mesozoic and during the Cenozoic (López Ramos, 1979; Keppie *et al.*, 2011). The Yucatán block evolution is linked to the opening of the Gulf of

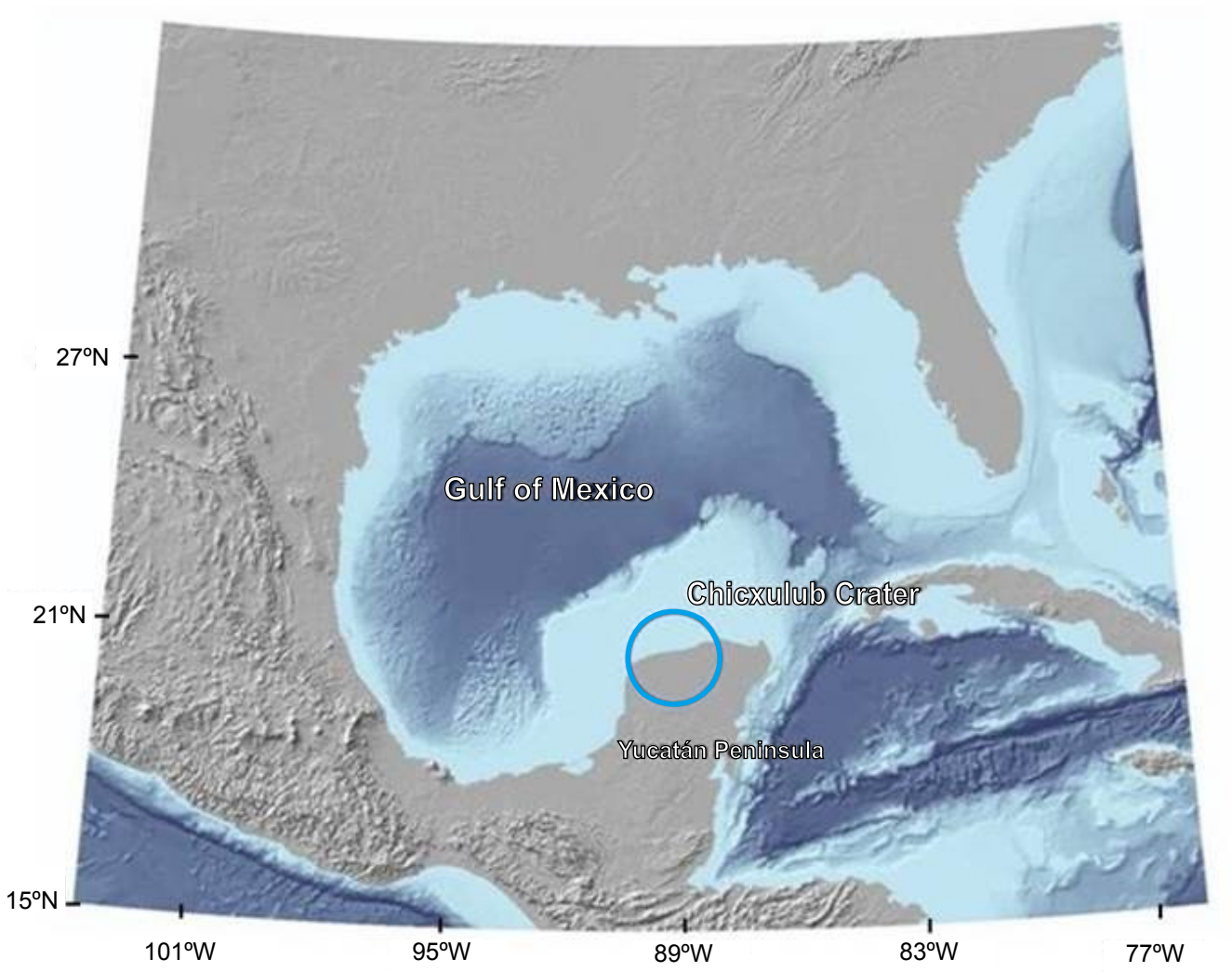

FIGURE 1. Map of Gulf of Mexico showing the location of the Chicxulub impact crater in the Yucatán Peninsula, modified from French and Schenk (2004).

Mexico and Caribbean Sea since the middle Jurassic (Pindell and Dewey, 1982; Molina-Garza *et al.*, 1992; Marton and Buffler, 1994; Bird *et al.*, 2005) involving tectonic displacements during the opening of the gulf and subsequent subsidence/uplift. Absence of outcrops of Mesozoic and Paleogene strata in northern Yucatán Peninsula has limited the completeness of stratigraphic studies, which are mainly based on borehole data and geophysical surveys (López Ramos, 1976, 1979). Carbonate sedimentation and depositional conditions on the platform have been controlled by tectonics, climate and sea level changes. In the northwestern Yucatán area, platform sedimentation conditions changed with the formation of Chicxulub Crater Basin, permitting the accumulation of thick sequences during the Paleogene (Bell *et al.*, 2004; Whalen *et al.*, 2014).

Seismic attribute analysis is a widely used technique in oil exploration, providing quantitative and qualitative petrophysical characterization and stratigraphic and structural information on sedimentary basins and hydrocarbon reservoirs (Taner *et al.*, 1979; Chopra and Marfurt, 2005, 2008). Complex trace attribute analyses allow mapping of subtle seismic impedance changes, in turn useful for petrophysical characterization and structural/stratigraphic mapping of package thickness and geometry, facies changes and discontinuities due to faults and fractures. Seismic attribute analysis has not been used to interprete the seismic data on the Chicxulub Crater, except for a previous preliminary analysis (Salguero-Hernández *et al.*, 2010).

The objectives of this study are to investigate the structure and stratigraphy of the impact breccias, the crater floor marked by the contact between the breccia and basal carbonate sediments and the post-impact carbonate sequence. The interpretation is based on seismic images and the attribute analysis on a grid of 19 seismic profiles in the crater marine central sector.

Chicxulub Crater

The Chicxulub Crater Basin, located in the Yucatán Platform, southern Gulf of Mexico (Fig. 1), formed as a result of a large asteroid impact at the K/Pg boundary (Hildebrand *et al.*, 1991; Schulte *et al.*, 2010). The impact created a ~200km rim diameter complex crater, forming a large depositional basin in the platform (Morgan *et al.*, 1997; Gulick *et al.*, 2008). The crater multi-ring morphology can be observed in the semi-circular concentric gravity anomaly pattern with a central gravity high and in the seismic reflection profiles (Sharpton *et al.*, 1993; Morgan *et al.*, 1997) (Fig. 2A). Major structural elements are depicted in a schematic cross-section (Fig. 2B), with the central basement uplift, fault system, terrace zone, displaced/deformed target rocks, impact melt rocks, peak ring and post-impact carbonate sediments. The crater is presently located part on land and part offshore, with its geometric center in the Yucatán coastline at Chicxulub Puerto. The crater has been investigated with an array of geophysical methods and drilling programs (*e.g.* Penfield and Camargo-Zanoguera, 1981; Hildebrand *et al.*, 1991, 1998; Sharpton *et al.*, 1993; Pilkington *et al.*, 1994; Urrutia-Fucugauchi *et al.*, 1996, 2004, 2008; Morgan *et al.*, 1997, 2005; Gulick *et al.*, 2008, 2013; Schulte *et al.*, 2010; Batista *et al.*, 2013).

Penfield and Camargo-Zanoguera (1981) used combined analysis of gravimetric and aeromagnetic data and borehole logs to interpret the geophysical and borehole information, with the occurrence of the "andesitic igneous zone" as a possible impact crater. Successive studies confirmed the impact origin and K/Pg age of Chicxulub (Hildebrand *et al.*, 1991, 1998; Sharpton *et al.*, 1992, 1993; Urrutia-Fucugauchi *et al.*, 1996, 2011). Analyses of potential field anomalies and seismic reflection profiles reveled a central structure characterized by a peak ring and central uplift with concentric internal and external rings (Sharpton *et al.*, 1993; Connors *et al.*, 1996; Morgan *et al.*, 1997; Hildebrand *et al.*, 1998 ; Vermeesch and Morgan, 2008). Since the 1990's, the Chicxulub Crater has received renewed attention from the scientific community interested in the mass extinction and K/Pg boundary events. The effects of the impact on the climate and life support systems have been considered the major cause of the end Cretaceous extinction (Alvarez *et al.*, 1980; Schulte *et al.*, 2010).

Geologic mapping shows that most of the peninsular northern and eastern sectors are covered by Pliocene and Quaternary carbonates, with older Eocene and Paleocene units to the South (López Ramos, 1976, 1979). In the northern Yucatán Peninsula, the Paleogene sedimentary sequence has been investigated by drilling as part of the PeMex exploration program and more recently by the Universidad Nacional Autónoma de México (UNAM), International Continental Drilling Program (ICDP) and International Ocean Discovery Program (IODP) (Fig. 3). The Pemex drilling program provided the first direct evidence of the impact breccias and melt rocks, which were sampled in boreholes at depths around 900 to 1100m in the central crater zone (Penfield and Camargo-Zanoguera, 1981; Hildebrand *et al.*, 1991; Urrutia-Fucugauchi *et al.*, 2011). Boreholes Chicxulub-1, Sacapuc-1 and Yucatán-6 penetrated a carbonate sequence and the underlying igneous-textured unit of andesitic composition (Fig. 3). The Pemex program incorporated intermittent coring,

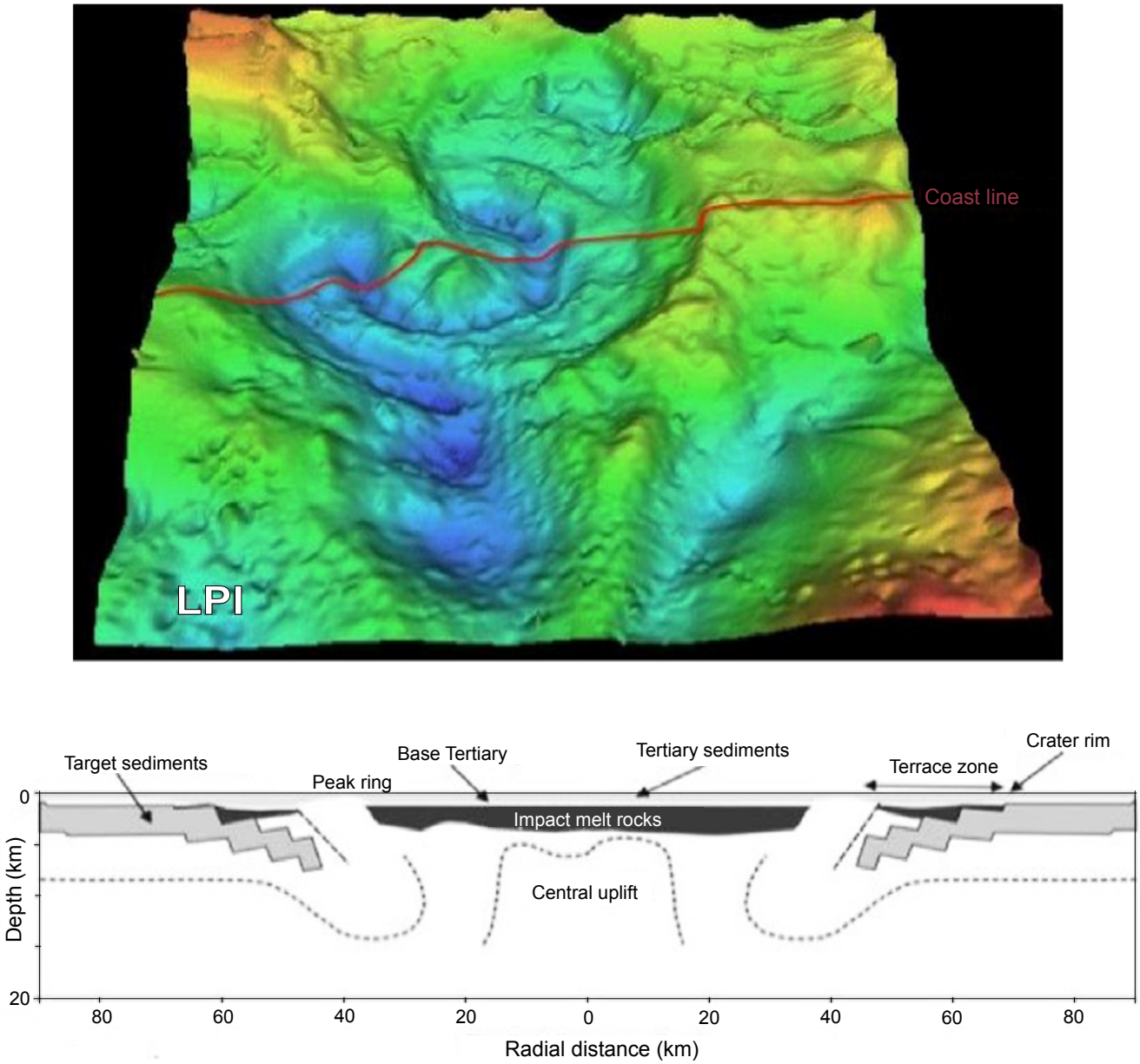

FIGURE 2. A) Bouguer gravity anomaly over the Chicxulub Crater (Sharpton *et al.*, 1993). B) Schematic cross-section of the Chicxulub Crater showing the major structural elements (Collins *et al.*, 2008).

which provided limited sampling of the different units. The UNAM drilling program incorporated continuous core recovery programs, permitting sampling the carbonate sediments at different sectors inside and around the crater zone (Urrutia-Fucugauchi *et al.*, 1996). Three boreholes in the southern zone, Santa Elena, Tekax and Peto boreholes, were drilled in the impact breccias of the proximal ejecta blanket. The central-eastern sector was further sampled in the Universidad Nacional Autónoma de México-Comisión Federal de Electricidad (UNAM-CFE) program, with the easternmost borehole reaching the impact breccias (Urrutia-Fucugauchi *et al.*, 2008). The terrace zone was drilled in the southern sector with the ICDP Yaxcopoil-1 (Yax-1) borehole, which provided a continuously cored section of post-impact carbonates, ~100m of impact breccias and a thick section of more than 1km of displaced Cretaceous carbonates (Urrutia-Fucugauchi *et al.*, 2004).

The UNAM exploration wells sampled the post-impact carbonate sequence and impact breccias. Boreholes Santa Elena (U5), Peto (U6) and Tekax (U7) cored the carbonate-breccia contact and the impactites, an upper breccia unit rich in melt and basement clasts and a lower breccia unit rich in carbonate clasts (Urrutia-

Fucugauchi *et al.*, 1996, 2011). The stratigraphy of two inverted breccia sequence resembles the suevitic and Bunte breccia units documented in the Ries Crater.

The IODP-ICDP Expedition 364 drilled the Chicx-03A borehole on top of the peak ring in the marine crater sector, sampling the post-impact carbonates, impactite units and peak ring sequence (Morgan *et al.*, 2016). The drilling program aimed to investigate the low-velocity zone that characterizes the peak ring and the annular gravity low. The borehole sampled a thick basement section of fractured granitic rocks lying at shallow depths, between ~748m and ~1335m below seafloor, beneath the peak ring. The occurrence of basement rocks supported peak ring formation models involving uplift of lower crustal material. It provided samples of the thickest basement section so far drilled. Basement rocks had been sampled earlier from clasts in the melt and basement rich breccias.

The crater sediment infill stratigraphy has been investigated in the seismic studies, initially along regional profiles across the marine sector of the structure as part of the 1996 British Institutions Reflection Profiling Syndicate (BIRPS) project (Morgan *et al.*, 1997; Snyder and Hobbs, 1999) and in a seismic grid in the 2005 Chicxulub Seismic Experiment (Gulick *et al.*, 2008, 2013). The BIRPS seismic reflection profiles imaged the crater basin and the deeper structure, with the crater floor morphology, peak ring, fault sets and underlying basement. The Chicxulub Seismic Experiment surveyed an area across the peak ring into the annular trough and the central zone. The two seismic surveys have provided data to investigate the shallow and deep structure beneath the Chicxulub Crater (Morgan *et al.*, 1997; Gulick *et al.*, 2008).

The BIRPS shallow seismic data have been re-processed and interpreted in subsequent studies, as the ~1km-deep basin with the post-impact sediment fill characterized by low velocities of around 2 to 3.5km/s (Brittan *et al.*, 1999). Bell *et al.* (2004) investigated the stratigraphy and depositional conditions inside the crater. In their

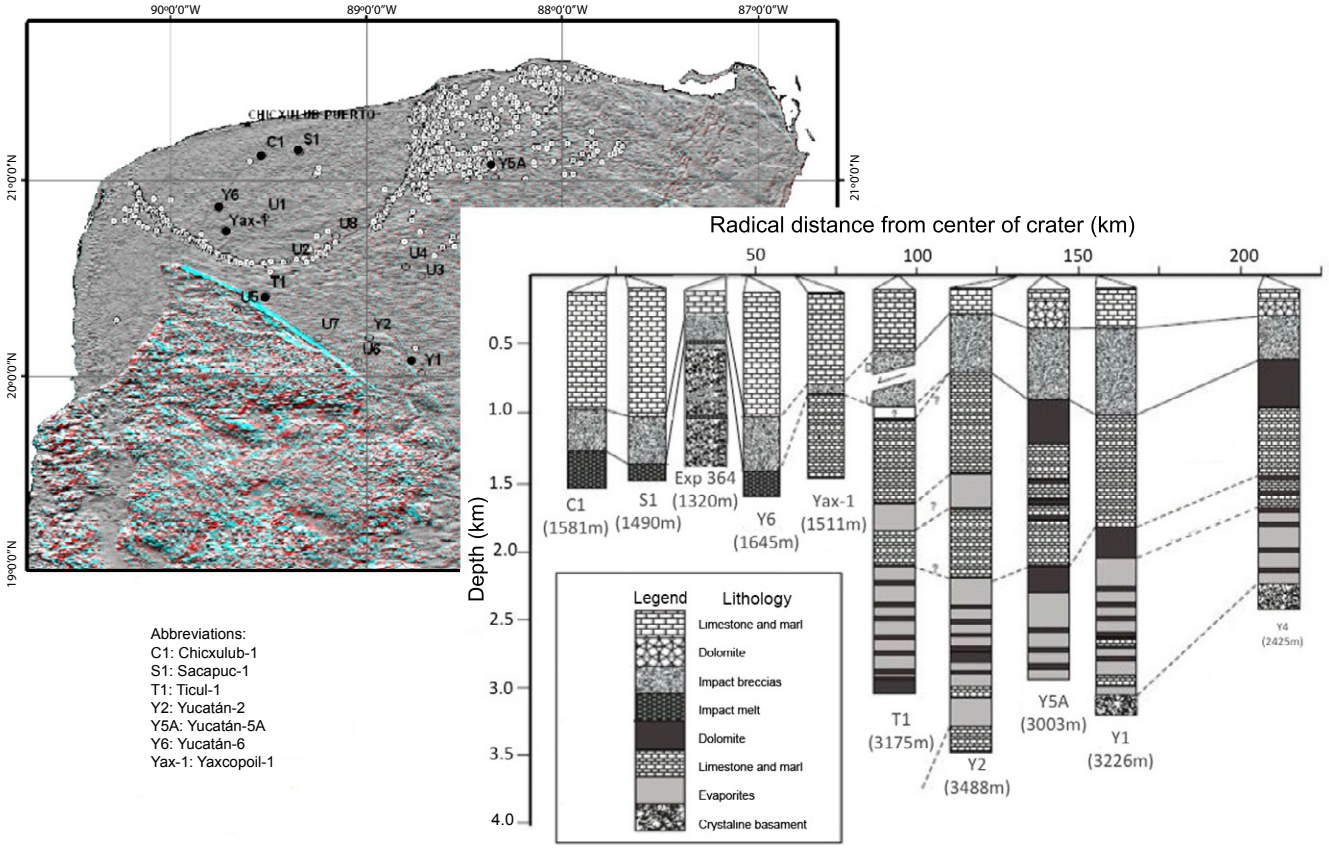

FIGURE 3. A) Location of drilling sites in the Chicxulub Crater and Yucatán area (Urrutia-Fucugauchi *et al.*, 2008, 2011; Morgan *et al.*, 2016). B) Schematic borehole columns for boreholes in the Yucatán Peninsula, across the Chicxulub Crater (adapted from López Ramos, 1979; Ward *et al.*, 1995; Rebolledo-Vieyra and Urrutia-Fucugauchi, 2004; Urrutia-Fucugauchi *et al.*, 2004; Morgan *et al.*, 2016).

study, stratigraphic packages were identified and mapped, reconstructing the gradual filling of the basin. The western and northwestern sectors were filled earlier than the eastern sector. The sedimentary packages are separated into a lower section and an upper section by a crater wide unconformity. The unconformity marks a major change in the depositional conditions, mainly in the eastern sector by a prograding shelf downlapping over the unconformity (Bell *et al.*, 2004). The clinoforms record a marine regression affecting the Yucatán Platform and the Chicxulub Basin (Whalen *et al.*, 2014).

The crater floor is characterized by relief marked by the elevated peak ring and the top surface of impact breccias (Gulick *et al.*, 2013). In the last stages of cratering during the collapse stage, tsunamis and backwash slides resulted in re-working and re-deposition of the breccias (Schulte *et al.*, 2010; Whalen *et al.*, 2014). The carbonate sequence was affected by hydrothermal alteration from the high temperature fluids and circulating sea water. Their long-lived effects are shown in geochemical logs of the Paleogene carbonates (Escobar-Sánchez and Urrutia-Fucugauchi, 2010). Their effects on the physical and chemical properties are discussed below in relation to the petrophysical characterization in the seismic attribute analysis. Heat from the melt maintained the active hydrothermal system, which lasted for more than a million years (Kring *et al.*, 2004; Escobar-Sánchez and Urrutia-Fucugauchi, 2010).

The Yucatán Platform has been described as a relatively undeformed low dipping ramp (Rosencrantz, 1990). The platform has evolved since the Early Cretaceous (Berriasian) after the rifting of the Yucatán tectonic block, with carbonate sediments deposited in this escarped rimmed platform (Wilson, 1975). Regional fault zones affect the eastern platform edge on the Caribbean Margin. The Campeche escarpment has been recently imaged from high-resolution multibeam bathymetric surveys, which have identified the impactite deposits exposed on the northern scarp (Paull *et al.*, 2014).

In our analyses, we concentrate on the carbonate sedimentary sequence below the unconformity, the upper breccias and the crater floor relief, with particular attention to the basal Paleogene sediments deposited in the basin, sediment transport and deposition over the peak ring and annular trough.

METHODS

The study area is located in the northern central sector of the Chicxulub Crater, in the Yucatán carbonate Platform. Marine seismic reflection surveys have been conducted for the oil exploration and for the Chicxulub projects. In this study, we analyze the seismic lines from the Chicxulub Seismic Experiment in the central crater sector (Fig. 4; Morgan *et al.*, 2005; Gulick *et al.*, 2008). Seismic lines were acquired in a dense profile grid (Table 1), which provided increased resolution in the central and annular sectors across the peak ring zone. Details of the survey design, acquisition parameters and processing are given in Gulick *et al.* (2008). To interpret the seismic lines, high-energy reflectors with lateral continuity were marked in the seismic images (Canales, 2013). Interpretation was based on the Petrel seismic simulation software (Schlumberger, version 2009) and the application of seismic attributes, 2-D line visualization, contour surfaces and 3-D oblique views for selected reflectors. The seismic images are plotted as a function of two-way travel time in milliseconds (ms).

Seismic attributes are used to investigate petrophysical properties within a seismic line grid and to infer rock types, small-scale structures and oil-gas-water interfaces (Chopra and Marfurt, 2005, 2008; Barnes, 2006; Liu and Marfurt, 2007). Seismic attributes are designed to enhance and extract information from measured seismic properties such as amplitude, frequency and lateral reflector continuity/discontinuities. We have determined the post-stack complex trace attributes of envelop amplitude, instantaneous phase, instantaneous frequency, Root Mean Square (RMS) amplitude and anelastic attenuation Q factor. Here we show the results for the cosine of phase and RMS attributes.

The cosine of phase, which represents a phase value (-1 to 1) signal associated with a point in time, is used to emphasize structural features. The phase corresponding to peaks, valley and zero crossings of the actual trace is assigned a given color (black or white), marking changes in the wavefront. The phase information is independent of the amplitudes of the traces, and although the events observed are weak, it serves to discriminate geometries and as indicator of lateral continuity, sample sequence boundaries and strata configuration.

The RMS attribute is determined as the square root of the sum of squared amplitudes normalized by the number of samples within a given $\{t_1–t_2\}$ interval. In the oil exploration seismic surveys, the RMS attribute is used as an indicator of hydrocarbon presence. The RMS amplitude is sensitive to random noise and it correlates with amplitude variance, reflection strength and average energy (Barnes, 2006).

SEISMIC INTERPRETATION

We analyze 14 seismic lines of the Chicxulub Seismic Experiment in the central sector (Fig. 4), three of which are segmented in seven lines, summing

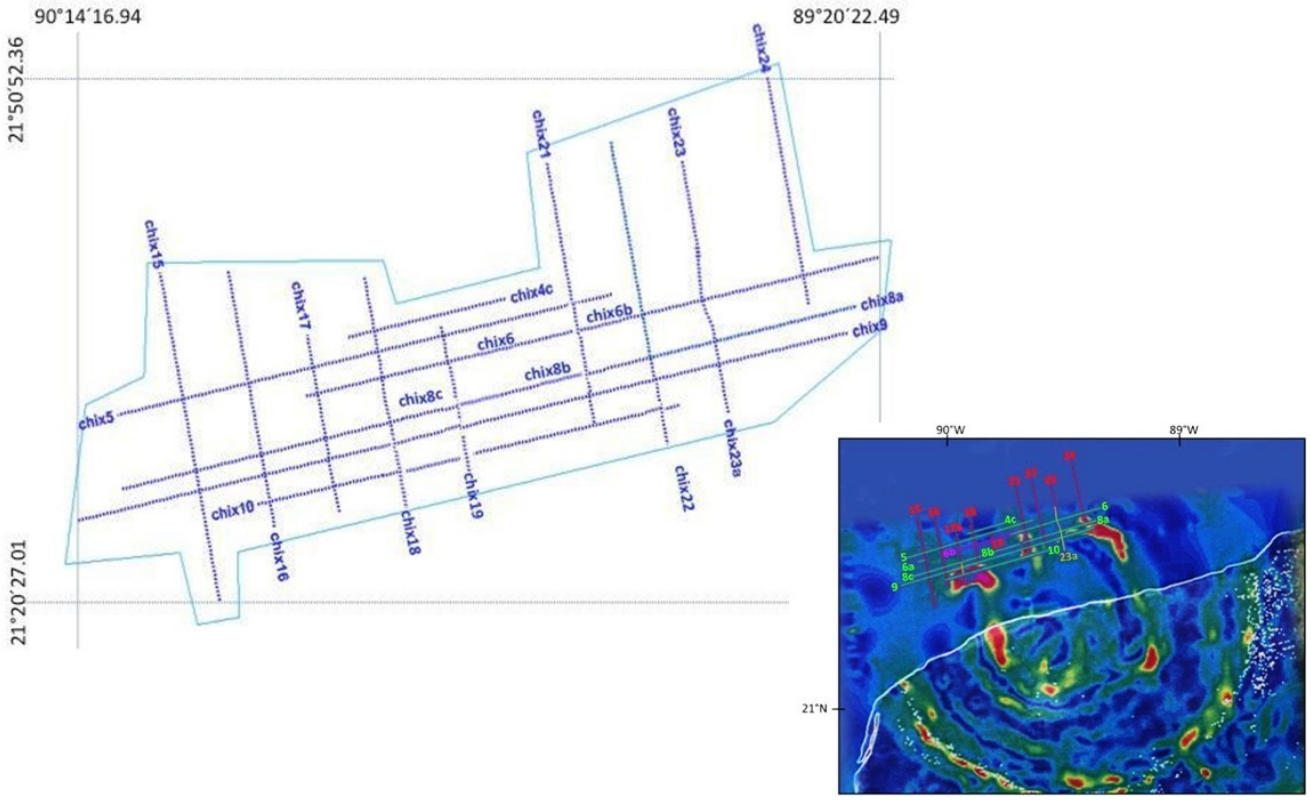

FIGURE 4. A) Location of the 19 seismic lines in the central sector of the crater. B) Horizontal gravity gradient of Chicxulub crater (Connors *et al.*, 1996), with the seismic lines.

up to a total of 19 seismic lines. Information on location, coordinates and length of seismic lines is summarized in Table 1. A total of 1822km of seismic reflection lines were acquired, including the central grid of high resolution profiles, which contains the 19 lines of this study, a semi-circular profile and three radial profiles (Gulick *et al.*, 2008). The R/V *Maurice Ewing* of the University of Columbia, equipped with a multichannel system with 6km streamer, and additionally, 28 ocean-bottom seismometers and 87 land seismometers were used for data acquisition in the project.

In this study, seismic reflections resulting from subsurface interfaces characterized by strong velocity and acoustic impedance contrasts were identified and marked in the profiles (Vail *et al.*, 1991; Christie-Blick and Driscoll, 1995). We considered that seismic properties, such as waveform, event amplitude, sequence patterns, depend on structural details, nature of interstitial fluids, as well as the absorption of frequencies of rock units located in the target strata and surface. The workflow is described below. Seismic data were loaded in the Petrel software and each line was accessed with the original data in separate interpretation windows.

Composite sections were constructed each one with two intersecting lines oriented approximately West-East and North-South (parallel and perpendicular to the coast line). Examples of the composite sections are presented in Figure 5A and 5B, corresponding to lines Chicx_16 and Chicx_10 and Chicx_15 and Chicx_9, respectively, in the western sector. Thickness variations are observed between the base of the crater horizon and the base of the breccias. Interpreted depth variations show reflectors that correlate across the grid and deepen South of the structure. These changes in the position of the proposed limits are reflected in isopach maps, which correlate with models of gravity anomalies (Sharpton *et al.*, 1993; Hildebrand *et al.*, 1998; Vermeesch and Morgan, 2008; Vermeesch *et al.*, 2009).

Packages with characteristic sets of reflectors are separated in the composite sections (Fig. 5). They are bounded by high-energy reflectors marked with different colors (pink, blue, green and yellow). The packages correspond to the upper breccia sequence, the basal sediments filling the basin bottom relief, the sediment section with basin-wide lateral continuity and an undifferentiated upper section, which is not analyzed in this study.

TABLE 1. Location, coordinates and length of the seismic profiles

Line	Latitude N	Longitude W	Total length (km)
4c	21°35'46.50	89°56'05.70	18.93
	21°37'58.70	89°45'25.91	
5	21°31'12.61	90°11'43.37	58.87
	21°38'13.37	89°38'20.51	
6b	21°32'18.45	89°58'57.30	29.93
	21°35'51.82	89°41'54.97	
6	21°35'16.89	89°45'05.36	43.60
	21°40'22.14	89°20'22.49	
8ª	21°33'23.82	89°41'15.20	34.40
	21°37'34.25	89°21'45.64	
8b	21°31'22.26	89°50'43.01	14.89
	21°33'08.11	89°42'16.98	
8c	21°26'55.17	90°11'20.47	33.52
	21°30'59.17	89°52'23.41	
9	21°25'06.14	90°14'16.94	91.81
	21°35'59.81	89°22'21.04	
10	21°26'01.90	90°02'14.59	49.69
	21°31'42.99	89°34'05.17	
15	21°39'28.37	90°08'49.47	35.72
	21°20'27.01	90°04'49.44	
16	21°39'32.54	90°04'11.81	27.9
	21°24'41.25	90°01'05.73	
17b	21°35'53.72	89°58'55.12	19.34
	21°25'37.18	89°56'43.46	
18	21°39'14.66	89°55'01.16	18.36
	21°29'28.19	89°52'58.50	
19	21°36'17.93	89°49'50.09	8.15
	21°31'58.43	89°48'54.93	
21	21°45'52.62	89°42'41.73	28.85
	21°30'47.57	89°39'31.57	
22	21°47'03.36	89°38'22.93	25.85
	21°33'19.16	89°35'27.76	
23a	21°40'58.97	89°32'35.97	18.42
	21°31'12.65	89°30'26.20	
23	21°45'59.72	89°33'34.01	10.55
	21°40'22.97	89°32'23.10	
24	21°50'52.36	89°27'48.05	24.85
	21°37'39.02	89°25'04.15	

The upper breccia sequence shows lateral variations in thickness. Its top boundary marked by the blue reflector delineates the relief of the basin floor, showing the topographic uplift of the peak ring. The basal sediments fill the basin floor relief and show lateral variations in thickness, with discontinuous reflectors. The lower limit of the upper breccia unit is less well defined, masked by the lack of resolution in the reflectors at those depths. The melt sheet is apparently restricted to the peak ring, with melt pockets in the annular trough as described in previous analysis and in the Yucatán-6 borehole (Barton *et al.*, 2010).

Results are presented in terms of surface contour maps for the marker reflectors in Figures 6 and 7. At travel times ranging between -500ms and -1300ms in the West-East direction, the pink reflector delimits the top of a package of discontinuous reflectors, interpreted as fractured or reworked materials (Fig. 6B). A fractured brecciated unit is a likely explanation for the pattern of discontinuous reflectors. Working upwards, a blue reflector is identified, with its travel times ranging between -450ms and -1000ms in a West-East direction (Fig. 7B; 6A). This reflector was chosen as the first relatively continuous present in every profile. Broken discontinuous reflectors of high amplitude can be observed below the blue reflector, but more continuous than those observed at greater depths in the fractured brecciated unit. Fractures or sedimentary discontinuities are therefore interpreted in the package located between the pink and blue horizons (Fig. 5A; B).

The basal package of reflectors (Chicx_B) is bounded at its base by a green horizon (Fig. 5A). Its depth ranges between -150m and -900m in a West-East direction. Its geometry is smoother than in the deeper reflectors, indicating that the shallower strata are less affected by variations in thickness. Upwards in the section, package Chicx_A is bounded by the colored green and yellow reflectors (Fig. 7B), and it ranges between -200m and -700m in a West-East direction. This package is relatively horizontal and its thickness increases towards the northeast. Its sediments appear deposited in low energy environments, allowing increasingly homogeneous distribution and thickness. At the basal sequence, relief of crater floor controlled the deposition of the basal carbonate sediments. These sediments form a relatively uniform unit with a seismic response characteristic of platform limestone sequences. Above the horizon marked in yellow, continuous high-amplitude reflectors are observed (Fig. 5). As already noted, reflectors in the section at approximately 200msm are nearly horizontal. In the overlying sedimentary unit above the unconformity (yellow reflector in the seismic profiles), no reflectors indicating young sequences are marked. This unit was not included in this study.

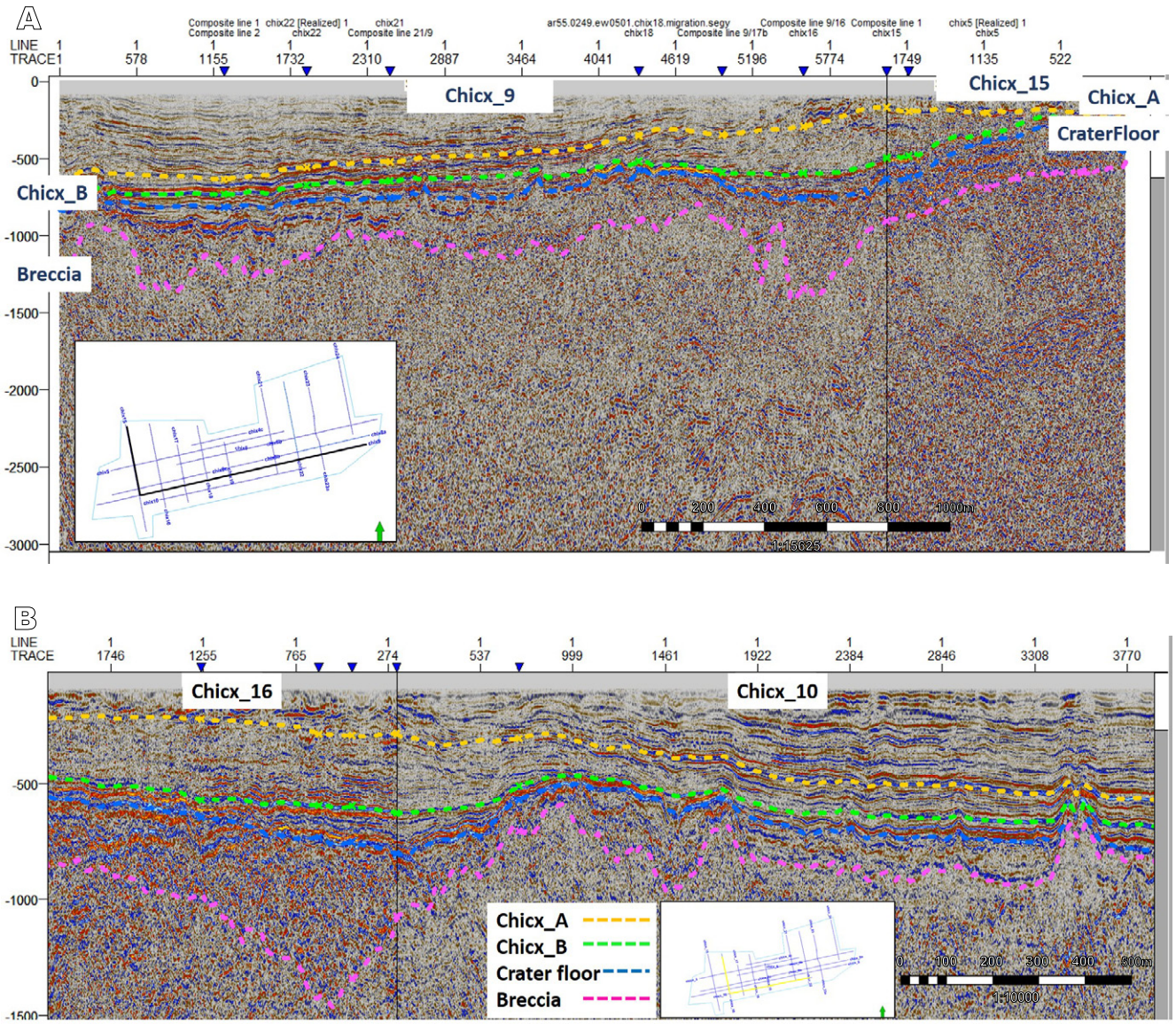

FIGURE 5. A) Composite section for lines Chicx_15, Chicx_9 showing the marked reflectors, the white boxes show the line position of lines (in black) in the seismic survey grid. B) Composite section for lines Chicx_16 and Chicx_10 showing the marked reflectors (in black).

In the analysis, stratigraphic packages are separated from their seismic response, in strata lateral continuity, signal amplitude, reflector amplitude and texture (Figs. 6 and 7). These properties are enhanced in the seismic attributes, highlighting contrasts in petrophysical properties. The cosine of phase and RMS attributes are used to further investigate lateral continuity of reflectors and reflector amplitudes.

In Figures 8 and 9, the joint analyses of the cosine of phase and RMS attributes for lines Chicx_5 and Chicx_9 are shown. The lines cross the structure in an E-W direction and show the geometry and inclination of the reflectors and package thickness variations from crater rim to the central zone, and the relief of the crater floor across the central zone and outside within the annular trough. The analysis of cosine of phase shows the distribution of the upper breccia package and the bathymetric relief of the basin floor (using the first laterally continuous reflector on top of the breccias). Chicx_A and Chicx_B packages are separated by high-energy continuous reflectors, showing the package lateral thickness variations. Seismic lines across the peak ring show changes associated with the bathymetry. The thickness of the breccia units is greater in the NW-SE lines in the annular through outside the elevated peak ring.

DISCUSSION

The stratigraphy of the crater central zone was investigated by the analyses of a grid of 19 seismic reflection profiles

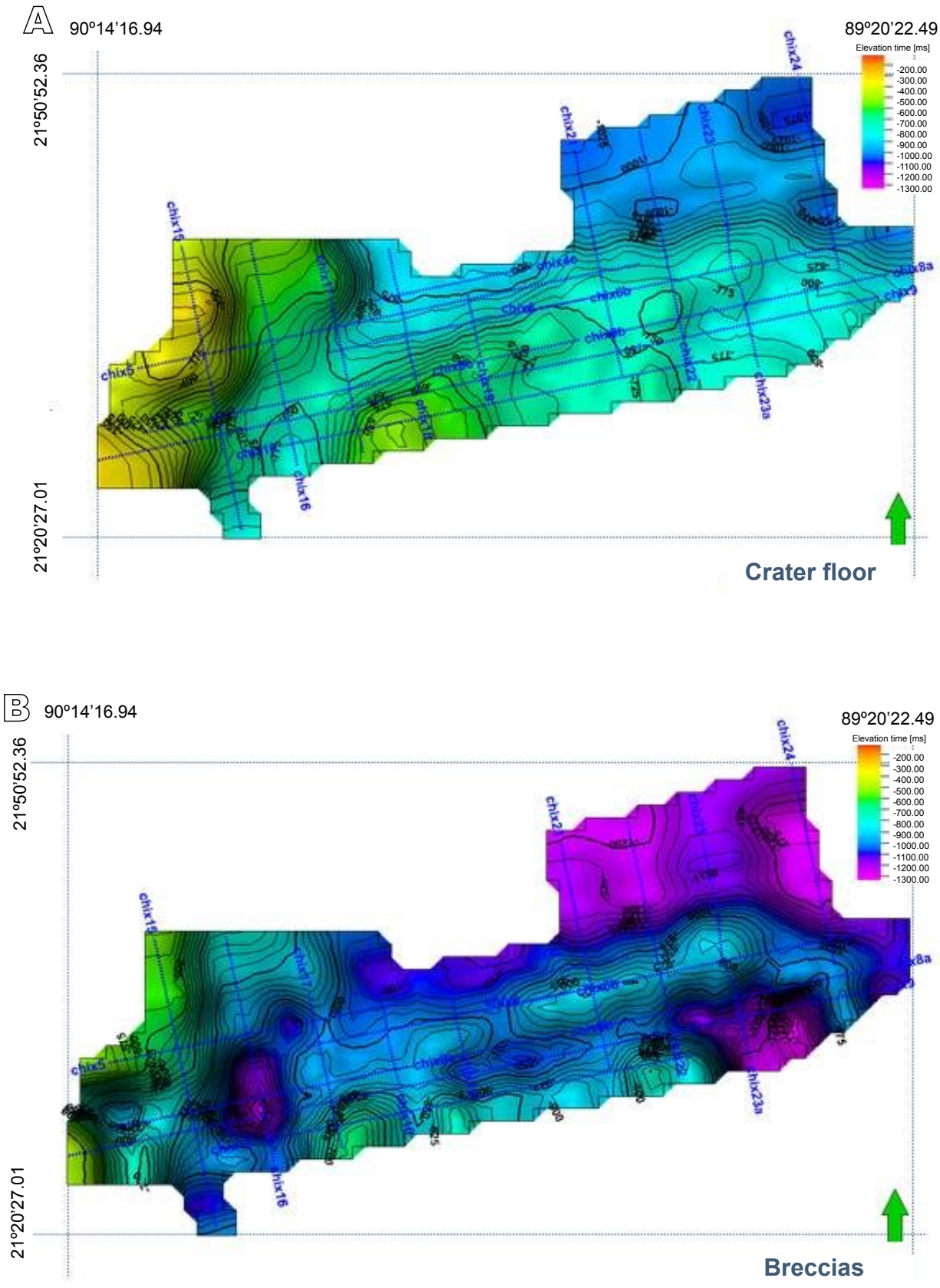

FIGURE 6. A) Surface contour map displaying the reflector interpreted as the base of the breccia package. It shows that the differences between depths measured through time varies from North to South. B) Surface contour map showing the crater floor configuration, marked by the horizon colored in blue.

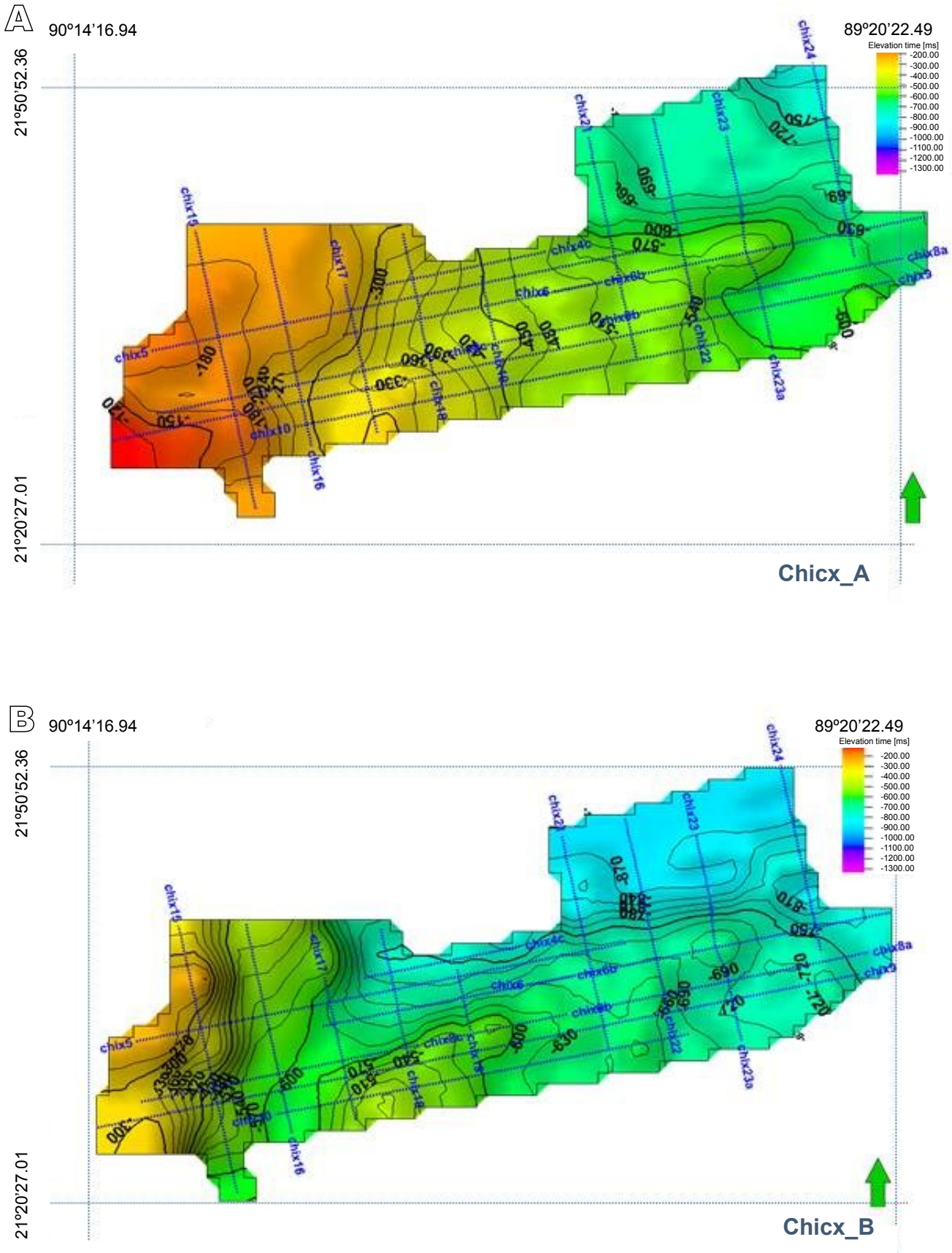

FIGURE 7. Surface contour maps for the post-impact Paleogene carbonate packages. A) Seismic package Chicx_A. B) Seismic package Chicx_B.

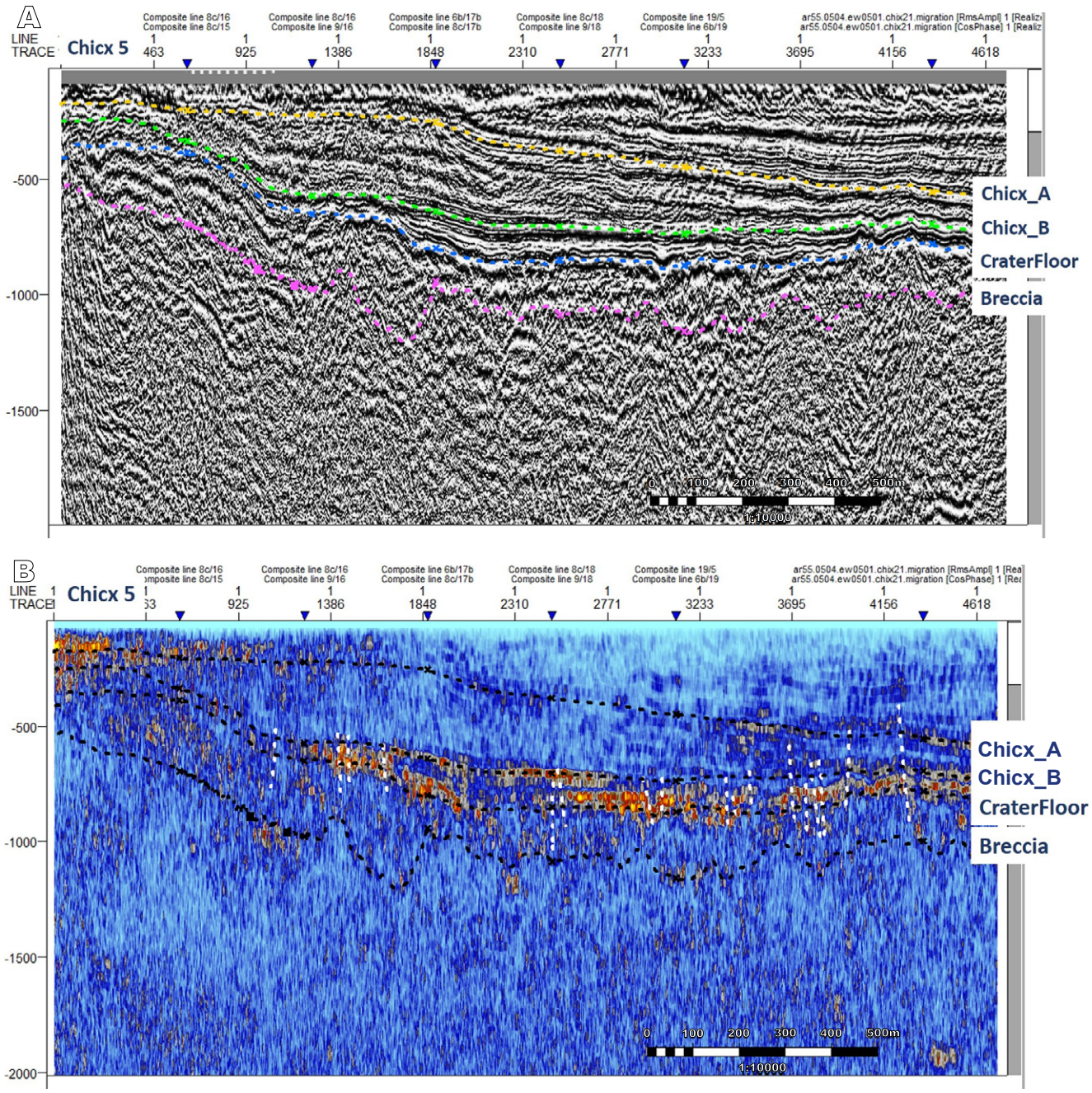

FIGURE 8. A) Cosine of phase for line Chicx_5. B) RMS attribute for line Chicx_5.

using seismic attributes, marker horizons, contour surfaces and 3-D views. Seismic units marked by high-energy laterally continuous reflectors are characterized, corresponding to the impact breccias and infill basal carbonates. The upper breccia unit has variable thickness with its top representing the crater basin floor. This marker horizon is represented by high-amplitude reflectors of the breccia-carbonate contact and a laterally continuous bottom reflector. The overlying basal carbonates with reflectors paralleling the basin floor relief is relatively thin; this unit is followed by a thicker unit with reflectors that gradually tending to the horizontal. These seismic stratigraphic units were further interpreted in the petrophysical and seismic attribute analysis.

The post-impact carbonate sediment sequence deposited in the crater basin has been investigated in marine seismic reflection surveys and in the boreholes drilled in the land sector (Morgan *et al.*, 1997; Brittan *et al.*, 1999; Snyder and Hobbs, 1999; Bell *et al.*, 2004; Urrutia-Fucugauchi *et al.*, 2004; Vermeesch *et al.*, 2009;

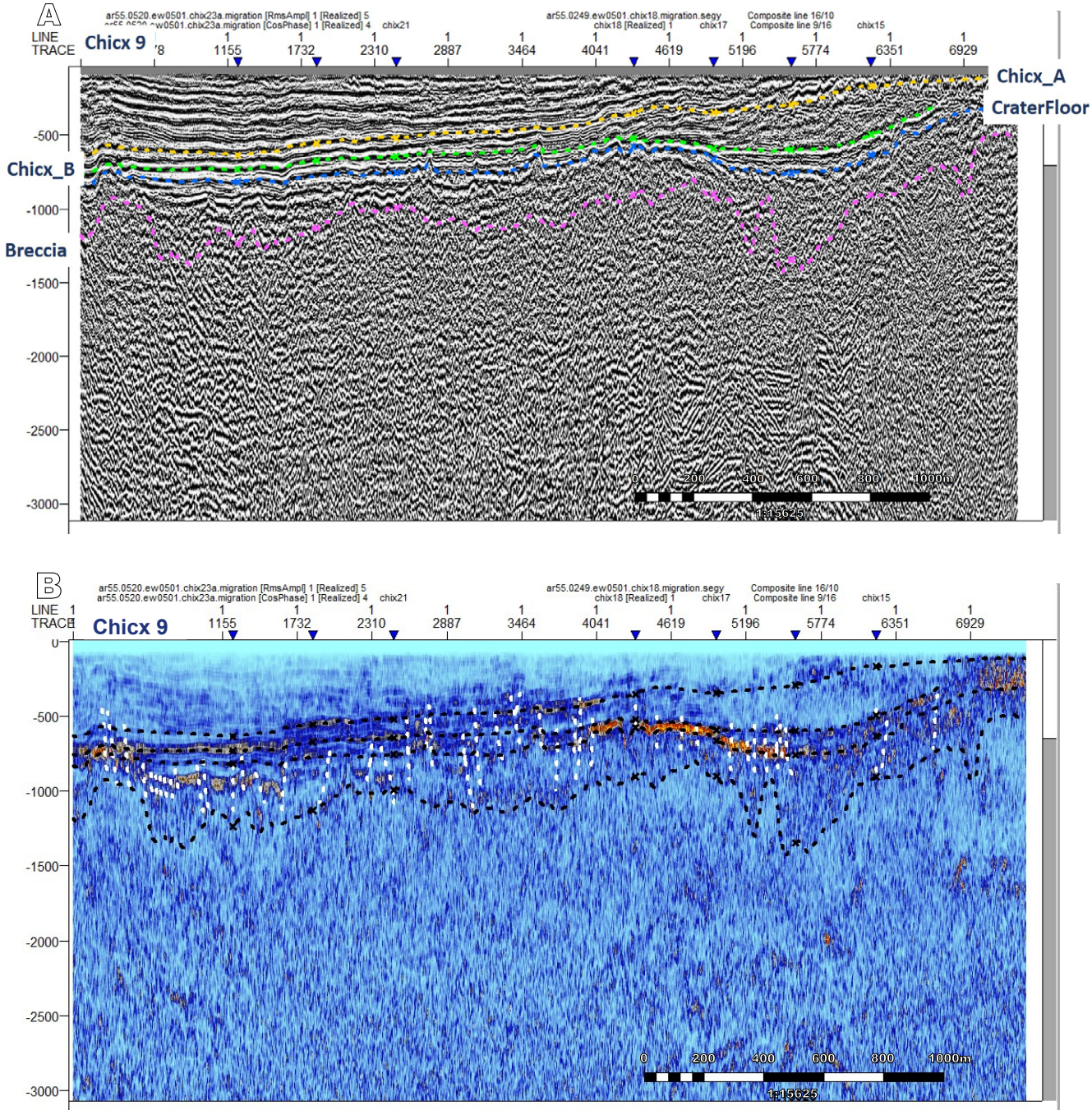

FIGURE 9. A) Cosine of phase for line Chicx_ 9. B) RMS attribute for line Chicx_9.

Gulick *et al.*, 2013; Whalen *et al.*, 2014). Bell *et al.* (2004) reported a stratigraphic analysis for some regional seismic reflection profiles from the 1996 Chicxulub seismic survey (Morgan *et al.*, 1997). Their analysis documents six different depositional packages characterized by distinct sets of reflectors separated by high energy reflectors. The depositional packages defined in Bell *et al.* (2004) and Whalen *et al.* (2014) were identified in our analysis, and extended laterally in the seismic profile grid of the central sector (Fig. 4). The analysis permitted us to document lateral changes in the thickness and distribution of the units, defined by the high-energy reflectors in the seismic profile grid. Results are summarized in terms of surface contour maps for the base of the breccia package and crater floor (Fig. 6) and for the Paleogene sediments (Chicx_A and Chicx_B packages) (Fig. 7).

The impact breccias are characterized as fragmented materials beneath the crater floor; the upper breccia package shows lateral variation in thickness with large

differences between the central and northern sectors. The reflector interpreted as the base of the breccia package varies from -500m to -1300m (Fig. 6A). In the seismic lines, packages of discontinuous reflectors characterize the fractured breccia unit. The bottom reflector limiting the upper breccia unit might represent the contact with top of the melt rock unit, which appears limited to the peak ring zone (Barton *et al*., 2010).

The crater basin floor is marked by high-amplitude reflectors that delineate the contact between the upper impact breccias and the overlying post-impact carbonates (Fig. 6B). The Paleogene carbonate sequence is characterized by two packages of multiple reflectors with lateral continuity (Chicx_A and Chicx_B) (Fig. 7), which contrast with the seismic response of the underlying impact breccias and the pre-impact carbonate units near the impact crater.

In the profiles, the blue horizon is interpreted as the crater floor represents the first semi-continuous reflector at an average depth of -800m (Fig. 6). At the southern sector, the reflector gets shallower reaching 400msm to 450msm and deepen to the North until 1000msm to 1100msm. Seismic reflectors associated to the peak ring are also present. In the central sector, the horizontal gradient gravity anomaly (Connors *et al*., 1996; Hildebrand *et al*., 1998) marks positive anomalies which mark density contrasts across the peak ring zone. The peak ring stratigraphy was been investigated in the IODP-ICDP Expedition 364, that which drilled a thick granitic basement section beneath the peak ring (Morgan *et al*., 2016).

Further characterization of the stratigraphic units was made from the seismic attributes. The cosine of phase attribute permits the separation of reflector packages, showing the characteristic response of the reflectors in each package. Within the upper breccia package, a high-amplitude reflector with lateral continuity present beneath the crater floor reflector in blue, might mark presence of the melt rocks. The reflectors marked in green and yellow separate a package of nearly uniform parallel strata. In the package, the relief follows the bottom reflectors of basin floor (blue reflector). The strata on the central zone above the yellow reflector are characterized by continuous high amplitude reflectors. The yellow reflector dips towards the northeast. The green reflector follows the bottom relief of basin floor. The basal Paleocene package is characterized by high-amplitude discontinuous reflectors parallel to basin floor (Fig. 5A; B).

The units below the crater floor formed by the impact breccias and melt-rich units have been sampled in the exploration boreholes on land (Hildebrand *et al*., 1998; Urrutia-Fucugauchi *et al*., 2011). Reflectors are characterized by high amplitudes and restricted lateral continuity, associated with brecciation, fracturing and hydrothermal alteration. Lateral variations in the thickness of the breccia unit are shown in the surface contour map and 3-D oblique view (Fig. 10). In this section, a discontinuous reflector marked in pink separates an upper section from a deeper section with no apparent reflectors. Morgan *et al*. (2000) interpreted in the 1996 seismic lines a low-frequency reflector marked by rapid increase in velocity up to 5.5km/s as the top of the melt sheet. Barton *et al*. (2010) correlated this low-frequency reflector with the up concave reflectors arising from sills underlain by a ~2-3km thick layered zone. The top of this reflective layer seems to correspond to a nearly horizontal thin high velocity layer, ~0.7km thick at ~1.6–1.8km deep, which is identified from the refractions in the streamer data. Gulick *et al*. (2013) mapped the ~1.9km low-frequency reflectors and high-velocity zone in the central crater zone, suggesting that the melt sheet might extend within the central sector and up to the annular trough (Barton *et al*., 2010). The Chicx-03A borehole over the peak ring drilled a ~130m breccia section with melt fragments that overlie a thin clast-poor melt rocks (Morgan *et al*., 2016).

The configuration and lateral variation in thickness of the carbonate units Chicx_A and Chicx_B are shown in the 3-D oblique views (Fig. 11). The 3-D model (Fig. 11) shows that the thickness of the basal Chicx_B package increases northwards. Above the lower sequence Chicx_A that forms the basal Paleocene section, the packages are characterized by sequences of parallel reflectors with lateral continuity in Chicx_B. Within the packages, reflectors delineate development of small basins and topographic highs and smaller abrupt peaks. The surface contour map for the Chicx_A reflector shows the differences between the central sector (in green) and the annular trough (shown in blue and green-yellow), with depths varying from -150m to -900m (Fig. 7). The configuration of the Chicx_A surface follows the relief of the crater floor (Fig. 6). The variations in thickness of the package correlate with the relief of the crater floor. The surface contour map for the Chicx_B reflector shows less relief, with semi-horizontal reflectors varying in depth between -200m and -700m from West to East. The surface maps for the sediment packages define the central zone and the annular trough.

In the analysis of the regional profiles A, A-1, B and C, Bell *et al*. (2004) identified five units marked by high-amplitude reflectors in the post-impact infill carbonates. The crater floor marking the contact between the breccias and the basal carbonates was marked by the bottom set of reflectors with lateral continuity. The lower reflector

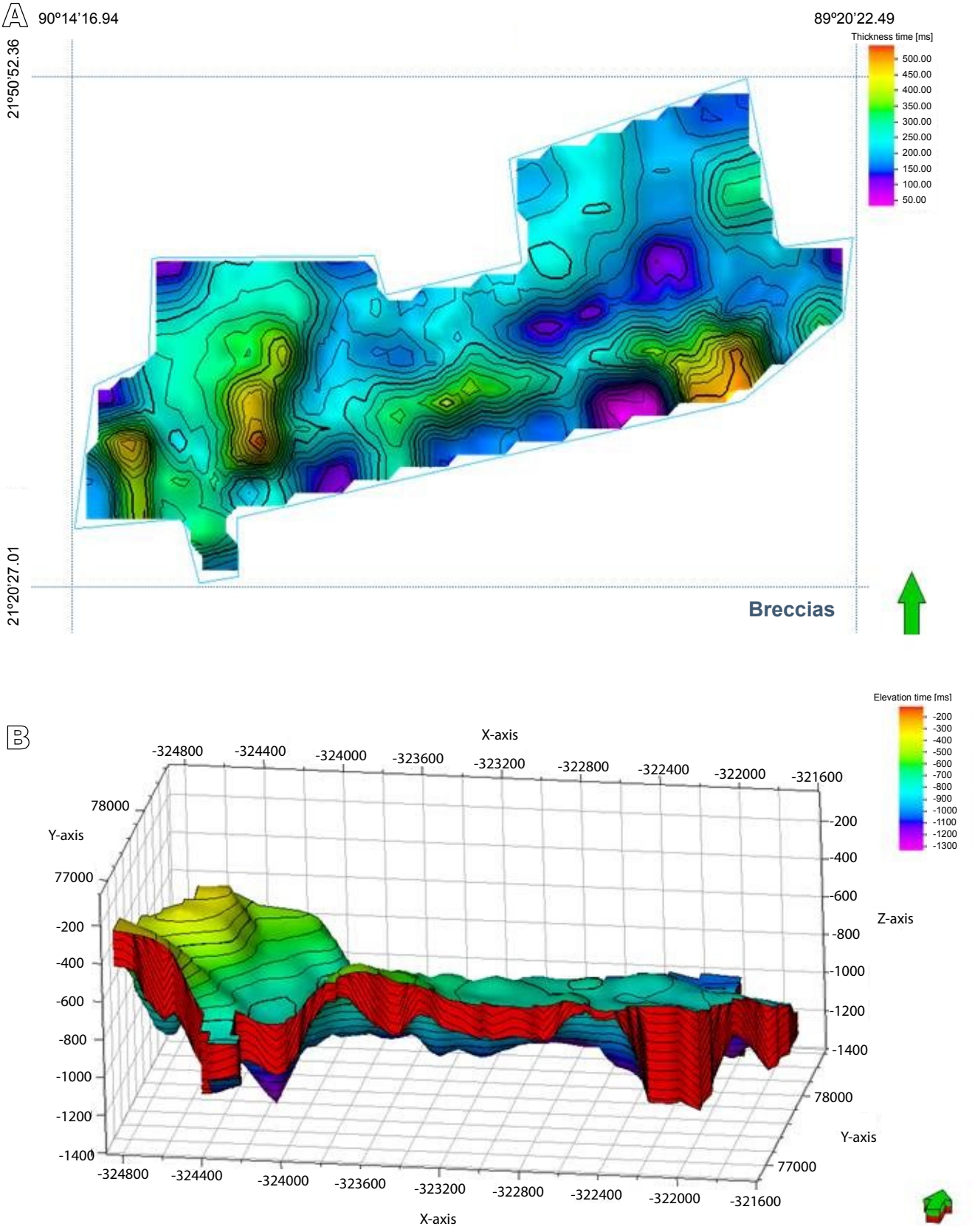

FIGURE 10. A) Isopach map illustrating the thickness of the breccia, between the breccia lower contact (pink) and crater floor (blue) horizons. B) 3-D oblique view of the upper breccia unit. Arrow on the side points to the North.

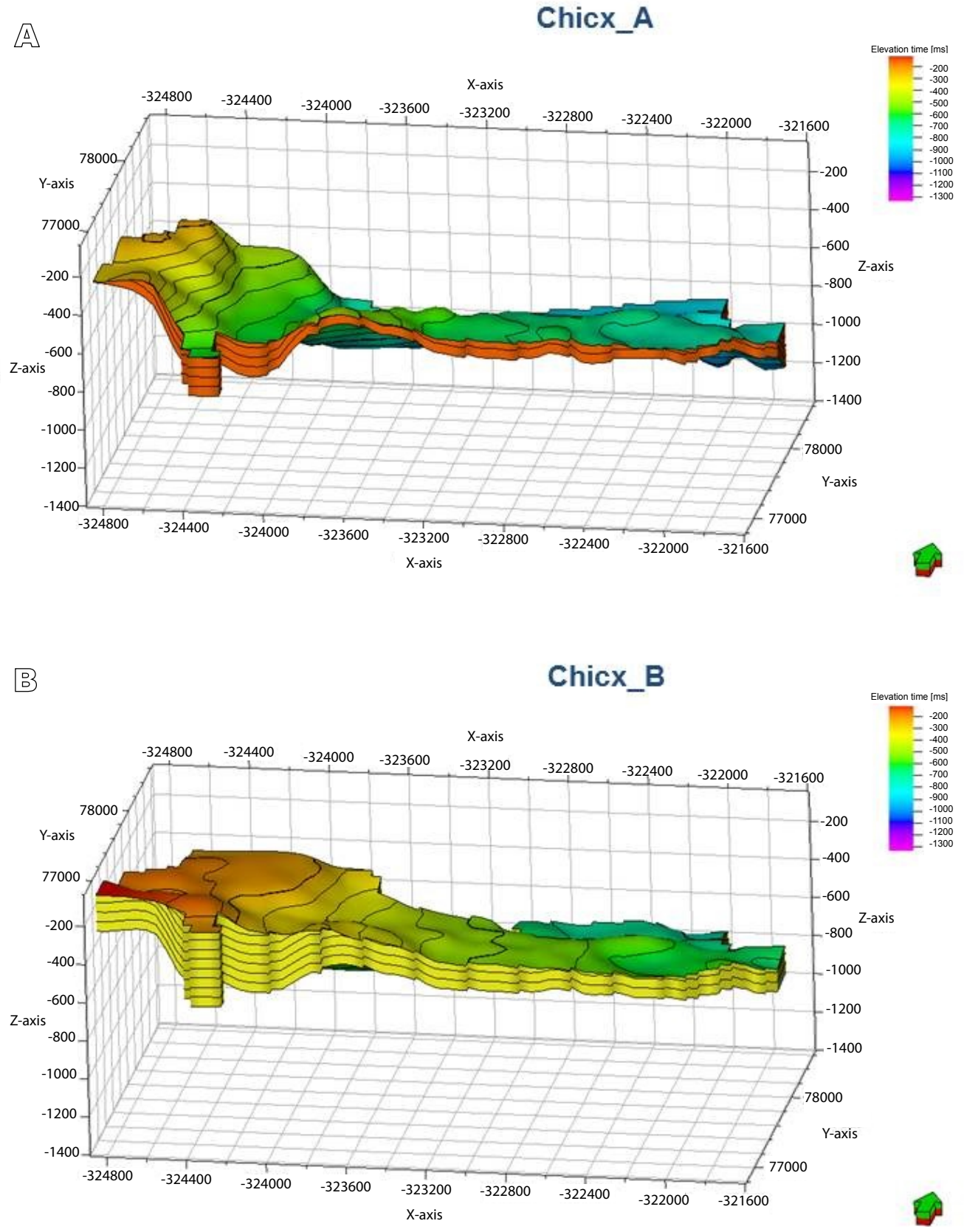

FIGURE 11. A) 3-D oblique view of basal sedimentary package Chicx_A. B) 3-D oblique view of sedimentary package Chicx_B. Arrow on the side points to the North.

was interpreted as the crater floor; however, as discussed in Bell *et al.* (2004) the upper reflector or somewhere in between could represent the contact of the impactite unit and basal carbonates. The basal Unit 1 forms the first set of continuous reflectors, which was divided into subunit 1a and 1b by the upper reflector that could represent the contact horizon. In the western section, reflectors onlap the higher energy reflector subdividing the subunits around a local bathymetric high. Unit 2 is characterized by an infill deposit that onlaps towards the peak ring high and the western basin end. Unit 3 is characterized by discontinuous low-amplitude set of reflectors that extends from reflectors parallel to the crater floor upwards into eastward 3-4 dipping clinoforms downlapping into a lateral continuous reflector. Bell *et al.* (2004) noted that thickness changes suggest a sediment source to the West, with slope progradation to the East. Unit 4 is characterized by high amplitude continuous reflectors that form eastward dipping clinoforms across the crater basin. Top of Unit 4 defines a depositional change, which in the eastern crater sector is marked by steep complex clinoforms recording a marine regression and which define a separate unit. Unit 5 defines a prograding slope with offlap forms controlled by lowering sea level. It is only present in the eastern sector, thinning to the West and overlap by a set of clinoform defined by shallow dipping 1-2 parallel reflectors, which represent the last depositional unit preserved or deposited in the marine crater sector (Unit 6).

Bell *et al.* (2004) discussed the depositional environments, history and relationships within the Yucatán Platform. They note that the regional unconformity formed during the Late Oligocene-Early Miocene could be represented the top reflectors marking Unit 4, which then implies an age around 23Ma for the prograding Unit 5. Alternatively, they note that the unconformities at the Paleocene-Eocene, Eocene-Oligocene and Middle-Upper Miocene boundaries might correlate with the lower part of Unit 5 regression package, then representing a younger age.

Whalen *et al.* (2014) analyzed the stratigraphy of the post-impact sediments cut in the Yaxcopoil-1 borehole. In the analysis, they distinguished 5 depositional units down to the contact with the impact breccias section at about 795m-depth. Based on a correlation with the P-wave velocity log (Popov *et al.*, 2004; Mayr *et al.*, 2007), Whalen *et al.* (2014) correlated the lithostratigraphic units to the seismic units of Bell *et al.* (2004). In their preferred correlation, they relate the lithostratigraphic units and the seismic units, with lithostratigraphic units 1 and 2 correlating with seismic Unit 1, lithostratigraphic units 3, 4 and 5 correlates with seismic Units 2, 3 and 4. In the lithostratigraphic column, Unit 1 is characterized by marly limestones and re-deposited carbonates. Unit 2 is characterized by argillaceous carbonates, with the top represented by re-deposited carbonates. Unit 3 is characterized by a thick carbonate sequence. Units 4 and 5 are formed by argillaceous carbonates. Unit 5 representing the marine regression marked by the complex clinoforms present in the eastern sector is grouped with the top Unit 6, defining the topmost depositional unit. The sections in the annular trough contain the thickest section of infill carbonate sediments (Bell *et al.*, 2004), which in the Yaxcopoil-1 borehole is represented by a section 795m thick. The Yaxcopoil-1 breccia section is ~100m-thick and is overlain by a carbonate megabreccia section. The breccia section has been subdivided into six subunits with distinct emplacement modes, with the upper subunit formed by reworked less consolidated breccias (Urrutia-Fucugauchi *et al.*, 2004; Kring *et al.*, 2004; Stöffler *et al.*, 2004).

In our analyses, the on-land boreholes are rotated to the position along the marine seismic lines assuming a radial symmetry, which allow to correlate borehole columns and geophysical logs to the marine seismic lines (Bell *et al.*, 2004; Whalen *et al.*, 2014). Studies have however uncovered asymmetries in crater structure and stratigraphy of impactites and sedimentary units (Gulick *et al.*, 2008, 2013; Ortiz-Aleman and Urrutia-Fucugauchi, 2010; Rebolledo-Vieyra *et al.*, 2010). The seismic stratigraphy analysis by Bell *et al.* (2004) shows the contrasts between the western and eastern sectors of sedimentary units, particularly in their Unit 4 above the unconformity. Whalen *et al.* (2014) proposed that the Yaxcopoil-1 borehole column correlates better with the sediment sequence on the eastern sector rather than with the western sector. These analyses emphasize the need for additional studies and in the case of the seismic data for mapping the reflectors and packages in surface contour maps and 3-D cubes.

Integrated 3-D cubes for the marker horizons defining the seismic units show the packages identified for the seismic units of the upper breccias, the Chicx_A basal sediment package and the Chicx_B sediment package (Fig. 12). The oblique views from the South and from the North show the variations in thickness and the configuration of the seismic units. Correlations of onland boreholes assuming radial symmetry need to be revised and constrained by additional data. The upper breccias (shown in red) are characterized by large variation in thickness. The basal sediments (shown in orange) follow the crater floor relief and get thinner over the bathymetric highs forming the crater floor. The overlying sediment package referred to as Chicx_B represents a thicker unit of infill sediments characterized by semi-horizontal strata.

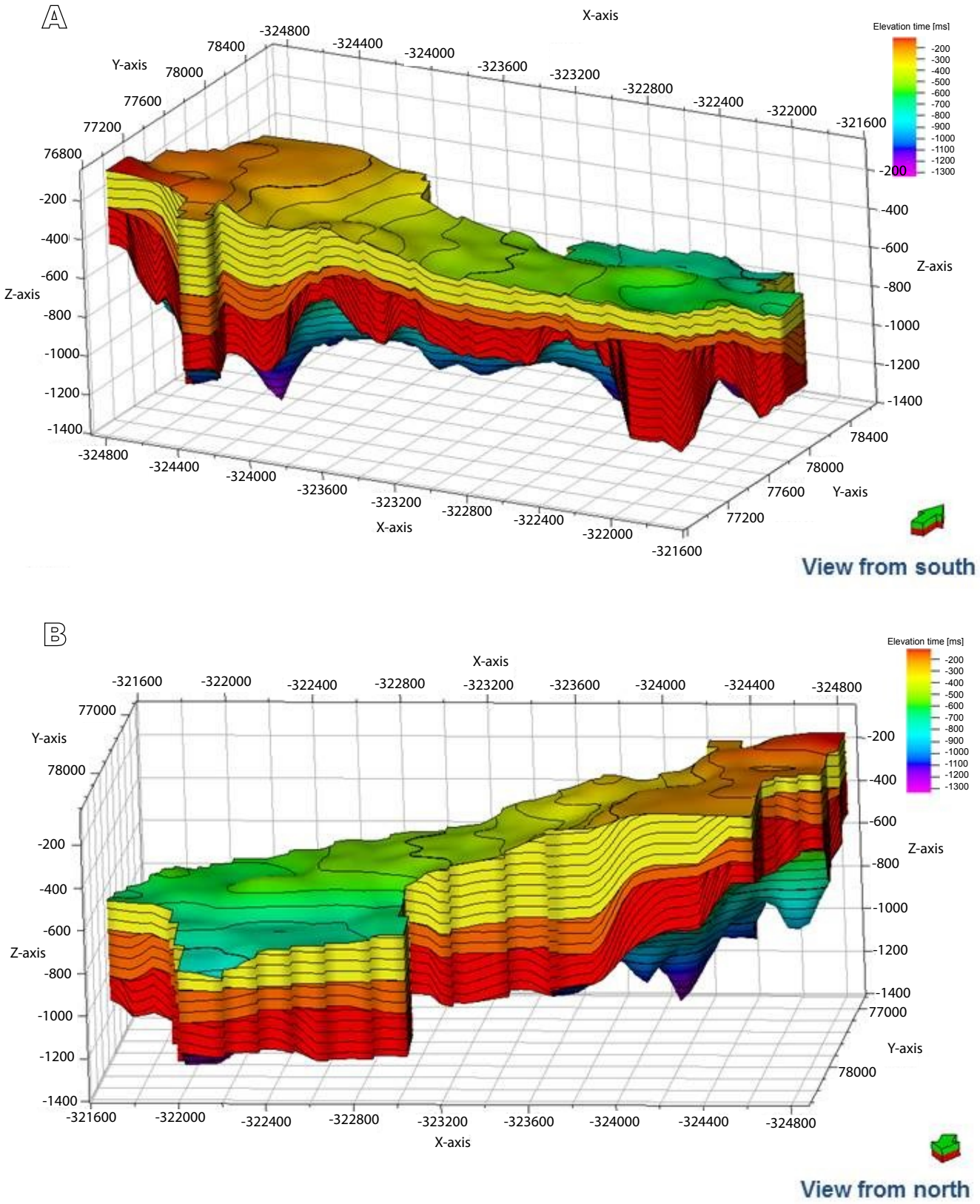

FIGURE 12. A) 3-D integrated oblique view from the South. B) 3-D integrated oblique view from the North. As already represented in Figures 10 and 11, the upper thicker (yellow) layer corresponds to Chicx_A, the thinner (orange) layer below this corresponds to Chicx_B, and the lower thick (red) layer are the Breccia.

CONCLUSIONS

A new stratigraphic interpretation of the impact breccia units and basal post-impact carbonate sediments in the Chicxulub central sector has been compared with previous analyses. Interpretation integrates seismic images and complex trace attribute analyses on a grid of 19 seismic reflection lines. The crater floor, marked by the contact between the impact breccias and the basal Paleocene carbonate sediments, is shown by laterally discontinuous high-amplitude reflectors at ~800msm. The crater floor, with the breccia-carbonate contact horizon, presents an irregular geometry probably associated with crater collapse and post-collapse action of tsunamis, gravity flows and faulting. The seismic signature of the breccias beneath the breccia-carbonate contact is characterized by laterally discontinuous reflectors. The base is marked by a high-amplitude reflector, which separates the units below characterized by a distinct impedance response with few reflectors. The reflectors above the top reflector of the breccia package are associated with the basal carbonate sediments deposited in the relief of the crater floor. The thickness of the breccia section varies between 570m to 120m, with an average thickness of ~400m.

Data integration in surface maps and 3-D cubes for the survey grid permitted to follow selected marker reflectors and to define the stratigraphic packages. Seismic attribute analysis allowed characterization of the carbonate sediments and impactites. Use of the cosine of phase and RMS attributes improved the definition of lateral continuity and the petrophysical characterization of seismic packages. The basal carbonates of Chicx_A units and upper breccia units are marked in the seismic attributes, showing the contrasts in petrophysical properties between the impactites and the carbonate sediments. The Chicx_A basal carbonates showed distinct petrophysical properties in the RMS attribute, which allowed higher definition in the stratigraphic analysis.

ACKNOWLEDGMENTS

Critical insightful comments by Gabriela Fernandez-Viejo, David Snyder, L. Perez-Cruz, the anonymous journal reviewers and section editor Puy Ayarza have been useful in revising the manuscript and are gratefully acknowledged. The study is based on the seismic data acquired by the Chicxulub Seismic Experiment (University of Texas at Austin Open-data repository). The Experiment was conducted as part of a joint project of University of Texas at Austin, the Imperial College Cambridge University and the Universidad Nacional Autónoma de México (UNAM). We thank I. Domínguez-Trejo, L. González-Mendoza, A. de J. Mendoza-Martínez, M.A. Díaz and M. Marca for their assistance. Thanks also to the Postgraduate course in Marine Science and Limnology at the UNAM. This study forms part of the Chicxulub Crater Research Program and UNAM Program for Continental and Ocean Drilling. Partial economic support for the study has been provided by a CONACYT scholarship to I. Canales-García and the UNAM PAPIIT IG-101115 grant.

REFERENCES

Alvarez, L.W., Alvarez, W., Asaro, F., Michel, H.V., 1980. Extraterrestrial cause for the Cretaceous-Tertiary extinction. Science, 208, 1095-1108.

Barnes, A., 2006. Too many seismic attributes? CSEG Recorder, 31(3), 41-45.

Barton, P.J., Grieve, R.A.F., Morgan, J.V., Surendra, A.T., Vermeesch, P.M., Christeson, G.L., Gulick, S.P.S., Warner, M.R., 2010. Seismic images of Chicxulub impact melt sheet and comparison with the Sudbury structure. Geological Society of America, Special Paper, 465, 103-113. DOI: 10.1130/2010.2465(07)

Batista, J., Pérez-Flores, M.A., Urrutia-Fucugauchi, J., 2013. Three-dimensional gravity modeling of Chicxulub Crater structure, constrained with marine seismic data and land boreholes. Earth Planets Space, 65, 973-983.

Bell, C., Morgan, J., Hampson, G.J., Trudgill, B., 2004. Stratigraphic and sedimentological observations from seismic data across the Chicxulub impact basin. Meteoritics and Planetary Science, 39, 1089-1098.

Bird, D.E., Hall, S.A., Burke, K., Casey, J.F., 2005. Gulf of Mexico tectonic history: Hot spot tracks, crustal boundaries and early salt distribution. American Association of Petroleum Geologists Bulletin, 89, 311-328.

Brittan, J., Morgan, J., Warner, M., Marin, L., 1999. Near-surface seismic expression of the Chicxulub impact crater. Geological Society of America, Special Paper, 339, 269-279.

Canales, I., 2013. Interpretación estructural y estratigráfica en perfiles sísmicos de reflexión del Cráter Chicxulub. Tesis Maestria en Ciencias, Programa Posgrado Ciencias del Mar y Limnología, Universidad Nacional Autónoma de México, 105pp.

Chopra, S., Marfurt, K.J., 2005. Seismic attributes – A historical perspective. Geophysics, 70, 3SO-28SO.

Chopra, S., Marfurt K.J., 2008. Emerging and future trends in seismic attributes. The Leading Edge, 298-318.

Christie-Blick, N., Driscoll, N.W., 1995. Sequence Stratigraphy. Annual Reviews Earth Planetary Sciences, 23, 451-78.

Collins, G.S., Morgan, J., Barton, P., Christeson, G.L., Gulick, S., Urrutia-Fucugauchi, J., Warner, M., Wünnemann, M., 2008. Dynamic modeling suggests terrace zone asymmetry in the Chicxulub crater is caused by target heterogeneity. Earth and Planetary Science Letters, 270, 221-230.

Connors M., Hildebrand, A.R., Pilkington, M., Ortiz-Aleman, C., Chavez, R.E., Urrutia-Fucugauchi, J., Graniel-Castro, E., Camara-Zi, A., Vazquez, J., Halpenny, J.F., 1996. Yucatán karst features and the size of Chicxulub crater. Geophysical Journal International, 127, F11-F14.

Escobar-Sánchez, J.E., Urrutia-Fucugauchi, J., 2010. Chicxulub crater post-impact hydrothermal activity - evidence from Paleocene carbonates in the Santa Elena borehole. Geofisica Internacional, 49, 97-106.

French, C.D., Schenk, C.J., 2004. Map showing geology, oil and gas fields, and geologic provinces of the Caribbean region. U.S. Geological Survey, Open-File Report 97-470-K. [CD-ROM]

Gulick, S., Barton, P., Christeson, G., Morgan, J., McDonald, M., Mendoza, K., Pearson, Z., Surendra, A., Urrutia-Fucugauchi, J., Vermeesch, P., Warner, M., 2008. Importance of pre-impact crustal structure for the asymmetry of the Chicxulub impact crater. Nature Geoscience, 1, 131-135. DOI: 10.1038/ngeo103

Gulick, S.P.S., Christeson, G.L., Barton, P.J., Grieve, R., Morgan, J., Urrutia-Fucugauchi, J., 2013. Geophysical characterization of the Chicxulub impact crater. Reviews of Geophysics, 51, 31-52. DOI: 10.1002/rog.20007

Hildebrand, A.R., Penfield, G.T., Kring, D.A., Pilkington, M., Camargo-Zanoguera, A., Jacobsen, S.B., Boynton, W.V., 1991. Chicxulub Crater: A possible Cretaceous/Tertiary boundary impact crater on the Yucatán Peninsula, Mexico. Geology, 19, 867-871.

Hildebrand, A.R., Pilkington, M., Ortiz-Aleman, C., Chavez, R.E., Urrutia-Fucugauchi, J., Connors, M., Graniel-Castro, E., Niehaus, D., 1998. Mapping Chicxulub crater structure with gravity and seismic reflection data. In: Graddy, M.M., Hutchinson, R., McCall, G.J.H., Rotherby, D.A. (eds.). Meteorites: Flux With Time and Impact Effects. Geological Society of London, Special Publications, 140, 155-176.

Keppie, J.D., Dostal, J., Norman, M., Urrutia-Fucugauchi, J., Grajales, M., 2011. Study of melt and a clast of 546Ma magmatic arc rocks in the 65Ma Chicxuub bolide breccia, northern Maya block, Mexico: Western limit of Ediacaran arc peripheral to northern Gondwana. Intternational Geology Review, 53, 1180-1193.

Kring, D.A., Horz, L., Zurcher, L., Urrutia-Fucugauchi, J., 2004. Impact lithologies and their emplacement in the Chicxulub impact crater: Initial results from the Chicxulub scientific drilling project, Yaxcopoil, Mexico. Meteoritics and Planetary Science, 39, 879-897.

Liu, J., Marfurt, K.J., 2007. Instantaneous spectral attributes to detect channels. Geophysics, 72(2), P23-P31.

López Ramos, E., 1976. Geological summary of the Yucatán peninsula. In: Nairn, A.E.M., Stehli, F.G. (eds.). The Ocean Basins and Margins, Volume 3: The Gulf of Mexico and the Caribbean, New York, Plenum, 257-282.

López Ramos, E., 1979. Geología de México. México: Instituto de Geología, Universidad Nacional Autónoma de México, Tomo 3, 445pp.

Marton, G., Buffler, R.T., 1994. Jurassic reconstruction of the Gulf of Mexico basin. International Geology Reviews, 36, 545-586.

Mayr, S. I., Burkhardt, H., Popov, Y., Wittmann, A., 2007. Estimation of hydraulic permeability considering the micro morphology of rocks of the borehole Yaxcopoil-1 (Impact crater Chicxulub, Mexico). International Journal of Earth Science, 97, 385-399.

Melosh, H.J., 1989. Impact Cratering: A Geologic Process. New York, Oxford University Press, 245pp.

Molina-Garza, R., Van der Voo, R., Urrutia-Fucugauchi, J., 1992. Paleomagnetism of the Chiapas massif, southern Mexico: Evidence for rotation of the Maya block and implications for the opening of the Gulf of Mexico. Geological Society of America Bulletin, 104, 1156-1168.

Morgan, J.V., Warner, M., Chicxulub Working Group, Brittan, J., Buffler, R., Camargo, A., Christeson, G., Denton, P., Hildebrand, A., Hobbs, R., Macintyre, H., Mackenzie, G., Maguire, P., Marin, L., Nakamura, Y., Pilkington, M., Sharpton, V., Snyder, D., Suarez, G., Trejo, A., 1997. Size and morphology of the Chicxulub impact crater. Nature, 390, 472-476.

Morgan, J.V., Warner, M.R., Collins, G.S., Melosh, H.J., Christeson, G.L., 2000. Peak ring formation in large impact craters: Geophysical constraints from Chicxulub. Earth Planetary Science Letters, 183, 347-354.

Morgan, J.V., Warner, M., Urrutia-Fucugauchi, J., Gulick, S., Christeson, G., Barton, P., Rebolledo-Vieyra, M., 2005. Chicxulub crater seismic survey prepares way for future drilling. EOS: Transactions of the American Geophysical Union, 86, 325-332.

Morgan, J.V., Gulick, S.P.S., Bralower, T., Chenot, E., Chriteson, G., Claeys, P., 2016. The formation of peak rings in large impact craters, Science, 354, 6314, 878-882. DOI: 10.1126/science.aah6561

Ortiz-Aleman, C., Urrutia-Fucugauchi, J., 2010. Aeromagnetic anomaly modeling of central zone structure and magnetic sources in the Chicxulub crater. Physics Earth Planetary Interiors, 179, 127-138. DOI: 10.1016/j.pepi.2010.01.007

Paull, C.K., Caress, D.W., Gwiazda, R., Urrutia-Fucugauchi, J., Rebolledo-Vieyra, M., Lundsten, E., Anderson, K., Sumner, E.J., 2014. Cretaceous-Paleogene boundary exposed: Campeche Escarpment, Gulf of Mexico. Marine Geology, 357, 392-400.

Penfield, G.T., Camargo-Zanoguera, A., 1981. Definition of a major igneous zone in the central Yucatán platform with aeromagnetics and gravity. In: Society of Exploration. Geophysicists Annual Meeting, Technical Program. Abstracts, 51st Annual Meeting, pg.: 37. [Abstract]

Pierazzo, E., Melosh, H.J., 2000. Understanding oblique impacts from experiments, observations, and modelling. Annual Review Earth Planetary Sciences, 28, 141-167.

Pilkington, M., Hildebrand, A.R., 2000. Three-dimensional magnetic imaging of the Chicxulub crater. Journal of Geophysical Research, 105, 23479-23491.

Pilkington. M., Hildebrand, A.R., Ortiz-Aleman, C., 1994. Gravity and magnetic field modeling and structure of the Chicxulub crater, Mexico. Journal of Geophysical Research, 99, 147-162.

Pindell, J.L., Dewey, J.F., 1982. Permo-Triassic reconstruction of western Pangea and the evolution of the Gulf of Mexico/Caribbean region. Tectonics, 1, 179-211.

Popov, Y., Romushkevic, R., Bayuk, I., Korobkov, D., Mayr, S., 2004. Physical properties of rocks from the upper part of the Yaxcopoil-1 drill hole, Chicxulub crater. Meteoritics & Planetary Science, 39, 799-812.

Rebolledo-Vieyra, M., Urrutia-Fucugauchi, J., 2004. Magnetostratigraphy of the impact breccias and post-impact carbonates from borehole Yaxcopoil-1, Chicxulub impact crater, Yucatán, Mexico. Meteoritics Planetary Science, 39, 821-830.

Rebolledo-Vieyra, M., Urrutia-Fucugauchi, J., Lopez-Loera, H., 2010. Aeromagnetic anomalies and structural model of the Chicxulub impact crater, Yucatán, Mexico. Revista Mexicana de Ciencias Geologicas, 27, 185-195.

Rosencrantz, E., 1990. Structure and tectonics of the Yucatán Basin, Caribbean Sea, as determined from seismic reflection studies. Tectonics, 9, 1037-1059.

Salguero-Hernández, E., Urrutia-Fucugauchi, J., Ramírez-Cruz, L., 2010. Fracturing and deformation in the Chicxulub crater - Complex trace analysis of instantaneous seismic attributes. Revista Mexicana de Ciencias Geológicas, 27(1), 175-184.

Schulte, P., Alegret, L., Arenilla, I., Arz, J.A., Barton, P.J., Bown, P.R., Bralower, T.J., Christeson, G.L., Claeys, P., Cockell, C.S., Collins, G.S., Deutsch, A., Goldin, T.J., Goto, K., Grajales-Nishimura, J.M., Grieve, R.A.F., Gulick, S.P.S., Johnson, K.R., Kiessling, W., Koeberl, C., Kring, D.A., MacLeod, K.G., Matsui, T., Melosh, J., Montanari, A., Morgan, J.V., Neal, C.R., Nichols, D.J., Norris, R.D., Pierazzo, E., Ravizza, R., Rebolledo-Vieyra, M., Reimold, W.U., Robin, R., Salge, T., Speijer, R.P., Sweet, A.R., Urrutia-Fucugauchi, J., Vajda, V., Whalen, M.T., Willumsen, P.S., 2010. The Chicxulub asteroid impact and mass extinction at the Cretaceous-Paleogene boundary. Science, 327, 1214-1218.

Sharpton, V.L., Dalrymple, G.B., Marin, L.E., Ryder, G., Shuaraytz, B.C., Urrutia-Fucugauchi, J., 1992. New links between the Chicxulub impact structure and the Cretaceous/Tertiary boundary. Nature, 359, 819-821.

Sharpton, V.L., Burke, K., Camargo-Zanoguera, A., Hall, S.A., Lee, S., Marin, L.E., Suarez, G., Quezada, J.M., Spudis, P.D., Urrutia-Fucugauchi, J., 1993. Chicxulub multiring impact basin: Size and other characteristics derived from gravity analysis. Science, 261, 1564-1567.

Snyder, D.B., Hobbs, R.W., 1999. Deep seismic reflection profiles across the Chicxulub Crater. In: Dressler, B.O., Sharpton, V.L. (eds.), Large Meteorite Impacts and Planetary Evolution. Geological Society of America, Special Paper, 339, 263-268.

Stöffler, D., Artemieva, N.A., Ivanov, B.A., Hecht, L., Kenkmann, T., Schmitt, R.F., Tagle, R.A., Wittmann, A., 2004. Origin and emplacement of the impact formation at Chicxulub, Mexico as revealed by the ICDP deep drilling at Yaxcopoil-1 and by numerical modeling. Meteoritics and Planetary Science, 39, 1035-1067.

Taner, M.T., Koehler, F., Sheriff, R.E., 1979. Complex seismic trace analysis. Geophysics, 44(6), 1041-1063.

Urrutia-Fucugauchi, J., Pérez-Cruz, L., 2009. Multiring-forming large bolide impacts and evolution of planetary surfaces. International Geology Review, 51, 1079-1102.

Urrutia-Fucugauchi, J., Pérez-Cruz, L., 2016. Chicxulub asteroid impact: An extreme event at the Cretaceous/Paleogene boundary. American Geophysical Union Monograph, 214, 99-111.

Urrutia-Fucugauchi J., Marin, L., Trejo-Garcia, A., 1996. UNAM Scientific drilling program of Chicxulub impact structure: Evidence for a 300 kilometer crater diameter. Geophysical Research Letters, 23, 1565-1568.

Urrutia-Fucugauchi J., Soler-Arechalde A.M., Rebolledo-Viera M., Vera-Sánchez P., 2004. Paleomagnetic and rock magnetic study of the Yaxcopoil-1 impact breccia sequence, Chicxulub impact crater (Mexico). Meteoritics & Planetary Science, 39, 843-856.

Urrutia-Fucugauchi, J., Chávez J.M., Pérez-Cruz L., de la Rosa J.L., 2008. Impact ejecta and carbonate sequence in the eastern sector of Chicxulub crater. Comptes Rendus Geosciences, 341, 801-810. DOI:10.1016 /j.crte.2008.09.001

Urrutia-Fucugauchi J., Camargo-Zanoguera A., Pérez-Cruz L., Pérez-Cruz G., 2011. The Chicxulub multi-ring impact crater, Yucatán carbonate platform, Gulf of Mexico. Geofísica Internacional, 50, 99-127.

Vail, P.R., Audemard, F.E., Bowman, S.A., Eisner, P.N., Pérez-Cruz, G., 1991. The stratigraphic signatures of tectonics, eustasy and sedimentology: An overview. In Einsele, G., Ricken, W., Seilacher, A. (eds.). Cycles and Events in Stratigraphy. Springer-Verlag, 617-659.

Vermeesch, P.M., Morgan, J.V., 2008. Structural uplift the Chicxulub impact structure. Journal of Geophysical Research, 113, B7, B07103.

Vermeesch, P.M., Morgan, J.V., Christeson, G.L., Barton, P.J., Surendra, A., 2009. Three-dimensional joint inversion of travel and gravity data across the Chicxulub impact crater. Journal of Geophysical Research, 114, BO2105.

Ward, W., Keller, G., Stinnisbeck, W., Adatte, T., 1995. Yucatán subsurface stratigraphy Implications and constraints for the Chicxulub impact. Geology, 23, 873-876.

Whalen, M., Gulick, S., Pearson, Z., Norris, R.D., Pérez-Cruz, L., Urrutia-Fucugauchi, J., 2014. Annealing the Chicxulub impact: Paleogene Yucatán carbonate slope development in the Chicxulub impact basin, Mexico. Society for Sedimentary Geology, Special Publication, 105, 282-304. DOI:10.2110/sepmsp.105.04

Wilson, J.L., 1975. Carbonate Facies in Geologic History. Heidelberg, Berlin, Springer-Verlag, New York, 471pp.

Manuscript received April 2017;
revision accepted December 2017;
published Online May 2018.